INVESTIGATION OF THE UNSTEADY REVERSE FLOW AIRLOADS AT HIGH ADVANCE RATIOS

Graham Bowen-Davies
grahambd@umd.edu
Post Doctoral Research Assistant

Inderjit Chopra
chopra@umd.edu
Alfred Gessow Professor and Distinguished University Professor and Director

Alfred Gessow Rotorcraft Center
Department of Aerospace Engineering
University of Maryland, College Park, MD 20742

The comprehensive analysis UMARC has been modified to include a model for dynamic stall in the reverse flow region for high advance ratio helicopter. The reverse flow stall model adapts the Leishman-Beddoes dynamic stall model with concepts from a flat plate in accelerating flow. The model is evaluated against airloads data from the reverse flow region of the UH-60A slowed rotor test at high advance ratios between μ = 0.4–1.0. The dynamic stall model predicts dynamic stall in the reverse flow for all the test cases, but does not have a significant impact on the advancing side of the rotor. At lower advance ratios (μ = 0.4 and 0.6), the azimuth of dynamic stall is well predicted and the correlation with the measured airloads in the reverse flow is improved. At μ = 1.0, the model predicts multiple vortex shedding, which are present in the test, but the phase agreement is not satisfactory.

Nomenclature

C_C	Chord force coefficient
$C_{l\alpha}$	Lift curve slope
C_N	Normal force coefficient, total
C_{NV}	Lift from leading edge vortex
C_N^C	Circulatory part of normal force
$C_N^N C$	Non-circulatory part of normal force
$C_{N_{max}}$	Maximum normal force
C_N^{le}	Indicator for leading edge pressure
C_M	Pitching moment coefficient
C_P	Vortex center of pressure
C_V	Vortex lift increment
f	Trailing edge separation point
Kn	Kirchhoff separation parameter
M	Mach number
r	Dimensional radial station
R	Rotor radius
s	Distance in semi-chords
α_s	Shaft tilt (positive aft)
α_{eff}	Effective angle of attack
β	Compressibility factor
γ	Lock No.
μ	Advance ratio
ϕ	Wagner function
τ_v	Non-dimensional vortex time
θ_{75}	Collective
θ_{1s}	Longitudinal cyclic
θ_{1c}	Lateral cyclic

Presented at the 41st European Rotorcraft Forum, Munich, Germany, September 1-4, 2015.

1. INTRODUCTION

The objective of this paper is to investigate the unsteady aerodynamic environment in the reverse flow region of a high advance ratio rotor using an in-house comprehensive analysis. At high advance ratios, defined here as $\mu > 0.5$, the aeromechanics of the rotor have not been completely comprehended at this time. One of the key challenges that have arisen is to predict the so called dynamic stall in the reverse flow, which can have a large impact on rotor loads. In order to design the next generation of high-speed rotorcraft, the ability to predict this phenomenon is important.

Traditionally, helicopter maximum airspeed has been limited to less than 170 knots (μ of 0.4) by compressibility, dynamic stall and reverse flow aerodynamics causing high power requirements and exces-

sive vibrations. Future vertical lift requirements call for VTOL aircraft that are capable of cruise speeds in excess of 230 knots, a combat range of 400 km, 6K/95° high/hot hover capability and improved efficiency. These combined requirements cannot be met by existing helicopter technology; therefore, the industry is looking at alternative configurations including coaxial rotors, lift offset rotors, tilt-rotors and compound rotors often in conjunction with rotor rotational speed variation (reduction). As well as the technological challenges faced in achieving efficient rotor speed variation, there is a lack of understanding of the aeromechanics at high advance ratios and systematic validation of predictive capability.

Validation of prediction tools for reverse flow aerodynamics requires high quality test data at high advance ratios, which includes airloads measurements near the blade root. There have been several full-scale wind tunnel tests that have achieved high advance ratios with both powered and un-powered rotors[1]–[4]. These tests provided some valuable information for validation of integrated quantities (hub loads) by predictive tools[5]–[7]; however, none included airloads measurements or comprehensive blade loads data needed to investigate local aeromechanics.

In response to the need for detailed data at high advance ratios, there have been two recent wind tunnel tests that achieved high advance ratios. The first test was on the full-scale UH-60A rotor that was tested with its rotor slowed to 40% and 65% of nominal speeds at the U. S. National Full-Scale Aerodynamics Complex (NFAC)[8]. Datta, Yeo and Norman[9] provided a comprehensive evaluation of the results as well as a fundamental explanation of the reverse flow physics. The sectional pressure data showed evidence of unsteady aerodynamics in the reverse flow region at increasing advance ratios, characterized by a suction pressure peak moving from the trailing edge towards the leading edge. The integrated airloads data also showed a significant impulse in normal and chord force and pitching moment (with additional results available from Potsdam, Datta and Jayaraman[10]). This behavior was attributed to possible reverse flow dynamic stall. Several researchers have correlated comprehensive analyses with high advance performance data[11]–[15], sectional airloads data[13]–[15] and blade bending loads[11],[13]–[15]. Potsdam, Datta and Jayaraman[10] validated Helios/RCAS, a coupled Computational Fluid Dynamics-Computational Structural Dynamics solver (CFD-CSD), in the unique flow regime showing good agreement of global sectional airloads. The CFD analysis was able to predict a suction pressure peak moving towards the leading edge in the reverse flow; however, the overall magnitudes were not well predicted, which was attributed overly diffuse stall vortex prediction from insufficient grid resolution.

A second set of high advance ratio tests were carried out at the University of Maryland by Berry and Chopra[18]–[22] on a 4-bladed UH-60 like, Mach-scaled rotor ($1/9^{th}$ scale). The most recent tests have included a set of pressure sensors at 30% radial station so as to measure the reverse flow airloads and investigate the flow physics. The pressure data showed a suction peak in the reverse flow similar to the results of the full-scale test[9],[10]. Authors[16],[17] showed good correlation of performance at all advance ratios with low collectives. The preliminary results suggested that after the onset of reverse flow dynamic stall (seen in pressure data), the correlation of performance and loads degraded significantly.

Unsteadiness in the reverse flow leading to the separation of a leading edge stall vortex has been shown in two recent high advance ratio tests. The state-of-art in comprehensive analysis has not yet been shown to adequately predict these airloads. In order to predict these unsteady airloads satisfactorily, comprehensive analysis must incorporate appropriate unsteady models. Well known approaches to modeling unsteady airloads, such as the Leishman-Beddoes Dynamic Stall model[27],[28] and the ONERA model[23],[24] were not developed for such general applications as largely varying freestream velocity (flow reversal) including large angle of attack variations. Hence care must be taken to understand their limitations. CFD has the ability to model the unsteadiness, however, high resolution grids are required at computational cost.

The approach of this paper is to investigate the reverse flow aerodynamics of the UH-60A slowed rotor test by adapting the approach taken in the Leishman-Beddoes dynamic stall model. The model will be evaluated against sectional airloads data at 22.5% radial station. A brief description of the UH-60A slowed wind tunnel test is followed by an overview of the baseline Leishman-Beddoes model. The model description is then followed by a comparison with sectional airloads at four test conditions at advance ratios between 0.4 and 1.0.

2. DESCRIPTION OF UH-60A WIND TUNNEL TEST

A full-scale UH-60A rotor was tested in the U. S. National Full-Scale Aerodynamics Complex (NFAC) 40 by 80 ft wind tunnel at NASA Ames. Important properties of the rotor are listed in Table 1. The rotor was mounted on the NFAC Large Rotor Test Apparatus (LRTA) as shown in Fig. 1. A part of the testing included slowing the rotor to achieve high advance ratios. The test matrix included the conditions shown in Table 2. The rotor was set to 100%, 65% and 40%

Table 1. UH-60A blade properties.

100% RPM	258
Radius (ft)	26.833
Solidity	0.0826
Lock No. (γ)	7.0
Airfoil	SC1095 SC1094r8
Twist	-16°
Sweep	20° at 93%

Fig. 1. Full-scale UH-60A rotor installed on the Large Rotor Test Apparatus in the NFAC 40- by 80- ft wind tunnel.

Table 2. Test matrix for the UH-60A tests.

RPM Variation	40%, 65%, 100%
Shaft Angle (Degrees)	0°, 2°, 4° (aft)
Wind Speed (knots)	50 – 175
Collective (Degrees	0° – 8°
Advance Ratio	0.3 – 1.0

Table 3. Test data points investigated.

Point	M_{tip}	μ	C_T/σ	α_s	θ_{75}	θ_{1C}	θ_{1C}
9125	0.26	0.4	0.0722	0°	5.9°	1.70°	-6.50°
9145	0.26	0.6	0.0622	0°	7.9°	-0.27°	-10.08°
9162	0.26	0.9	0.0204	0°	0.0°	-3.95°	-0.29°
9175	0.26	1.0	0.0220	0°	1.94°	-5.11°	-2.74°

of nominal operating rotational speed (258 RPM) to achieve tip Mach number of 0.65, 0.42 and 0.26 respectively. The rotor shaft angle was set to 0°, 2° and 4° (aft). For each test condition, the collective was set and the cyclics were used to trim the rotor to zero first harmonic flapping measured at the blade root.

The comprehensive set of measurements included, in the rotating frame: nine stations of blade strain gauges (flapwise, chordwise and torsion) between 13.5% and 90% radius, eight stations of pressure measurement from 22.5% to 99% radius, pitch link loads and blade root deflections on all four blades. The fixed frame loads time history was measured and unique test points included blade deflection measurements and PIV. Only a limited subset of published data is available for correlation. The data points used to evaluate the dynamic stall model are shown in Table 3.

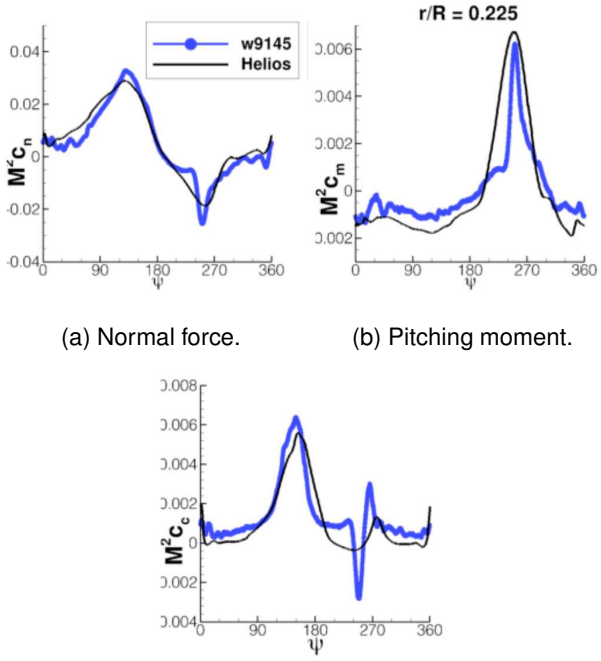

(a) Normal force. (b) Pitching moment.

(c) Chord force.

Fig. 2. Sectional airloads at 22.5% radius for test point 9145, μ = 0.6.

Figure 2 shows an example correlation of the current state in CFD-CSD predictions of reverse flow airloads (the results adapted from ref.[10]). The general agreement is good; however, focusing on the reverse flow region, the analysis is unable to predict the abrupt change in normal force near 240° azimuth and the associated chordwise impulse is not predicted. The peak pitching moment magnitude is well predicted, but the shape in the reverse flow is not well captured. It was suggested that CFD predictions may be improved with higher grid resolution, but a comprehensive (lifting line) analysis must rely

on empirical-based models to capture this behavior.

3.0 UMARC MODELING

The University of Maryland Advanced Rotor Code (UMARC)[25] was used as a baseline platform for this study. The blades are modeled as second order, nonlinear, isotropic, Euler-Bernoulli beams capable of 15 degrees of freedom that allow for coupled flap, lag, torsion, and axial motion. The equations of motion are solved using a variational methodology with modal reduction in conjunction with finite elements in space and time. 20 spatial elements and 12 time elements were used in this study, while 10 coupled blade modes are used in modal analysis. The lifting-line aerodynamic model implements quasi-steady aerodynamics by means of a table look-up for section lift, drag, and pitching moment coefficients. Near wake is modeled via a Weissinger-L representation and assumed to trail 30° behind the rotor in-plane from the trailing edge. The trailed wake is discretized into three azimuthal segments and the radial discretization is chosen to align with the aerodynamic discretization so as to minimize interpolation errors. The far-wake is modeled by the Bagai-Leishman relaxation free-wake model[26]. Convergence studies were conducted by evaluating the available sectional airloads data. A 15° azimuthal discretization of the wake with 2 turns of wake tracking gave satisfactory resolution at high advance ratios. The far-wake can be represented by an arbitrary number of wake trailers with increasing computational cost. In general, authors[17] have shown that at least two trailers at the blade tip are required to capture negative tip loading on a twisted rotor, and a root trailer improves airloads predictions on the rear of the rotor disk. Prior to this work, unsteady, attached airloads were modeled using the Leishman-Beddoes indicial attached flow model[29], but this was confined to outside of the reverse flow region andwas not applicable at very high advance ratios. This work extends the applicability to the reverse flow.

The wind tunnel test used fixed collective and zero first harmonic flapping at the blade root as the trim target and this approach was followed in the analysis. The nominal shaft angles are corrected to account for tunnel wall corrections. The coupled blade response and the root flapping constraints are solved iteratively to obtain the blade deflections and trim control settings.

4.0 REVERSE FLOW UNSTEADY MODELING

The helicopter rotor blade operates in an unsteady aerodynamic environment due to the 1/rev aerodynamic excitation of the rotor coupled with cyclic pitch variation, wake interaction and rotor dynamics. The shed wake induces a time varying inflow along the blade chord resulting in unsteady airloads. The unsteady airloads can be calculated numerically at high computational cost, or modeled approximately. For application in comprehensive analysis, an efficient unsteady model such as the Leishman-Beddoes indicial attached and dynamic stall models can be quite pertinent.

4.1 Overview of Leishman-Beddoes Attached Unsteady Model

The Leishman-Beddoes indicial model treats the unsteady loading of a pitching airfoil using the Wagner function (ϕ) to model the change in lift to a step change in forcing (α, $\dot{\alpha}$). Using superposition, the unsteady circulatory response to an arbitrary forcing can be determined,

$$C_N(s) = C_N(0) + \int_0^s C_{N\alpha}(M)\frac{d\alpha}{d\sigma}\phi(s-\sigma)\mathrm{d}\sigma \quad (1)$$

Here, s is the distance traveled by the airfoil in semi-chords. A similar approach is used to determine the unsteady circulatory response for pitching moment, as well as the response to pitch rate. Noncirculatory loads are derived from piston theory as described in Ref.[29]. The attached, compressible unsteady flow model is strictly two dimensional and in its original formulation was not suitable for varying freestream velocity. An example of the effect of the unsteady model on circulatory normal force is shown in Fig. 3 for a reduced frequency of 0.2. The model introduces a delay in the accumulation of lift. Jose and Leishman[30] reformulated the attached unsteady model in terms of circulation, rather than lift coefficient, to extend the models applicability to include varying freestream velocity (not including flow reversal) and showed reasonable correlation with 2D CFD results. A sample result of the circulatory normal force between the two approaches for a varying freestream is shown in Fig. 4. Including the freestream velocity has a significant effect after rapid flow decelerations such as happen on the retreating rotor disc and approaching reverse flow.

The efficiency of the unsteady calculation can be improved by approximating the integral in Eq. (1) with a recursive formulation and assuming finite differences for the differentials. The error is small for small enough time steps (ds). The resulting unsteady equation for the lift response to a change in angle of attack is given by:

$$C_N^C(s) = C_{n\alpha}(M)(\alpha_n - X_{1n}(s) - Y_{1n}(s)) \quad (2)$$

where

$$X_{1_n}(s) = X_{1_{n-1}}e^{-b_1\beta^2\Delta s} + A_1\Delta\alpha_n e^{-b_1\beta^2\Delta s/2}$$

$$Y_{1_n}(s) = Y_{1_{n-1}}e^{-b_2\beta^2\Delta s} + A_2\Delta\alpha_n e^{-b_2\beta^2\Delta s/2}$$

The approach has the advantage of not requiring storage of airloads from the entire time history (only $X_{1_{n-1}}$ is stored), although with modern computational power this may be less of a concern. However, this approach is more convenient for the Leishman-Beddoes dynamic stall model. Strictly speaking, the recursive approximation to the integral is not valid for large changes in freestream velocity and compressibility and this can introduce an error (Fig. 5), but for low Mach numbers such as are encountered in the reverse flow the error is expected to be small and can be neglected as shown in Fig. 6.

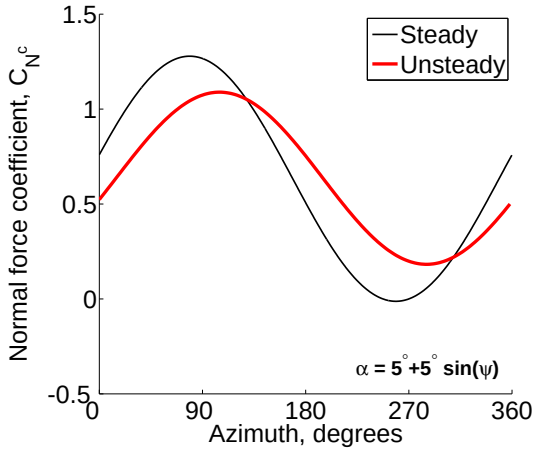

Fig. 3. Unsteady response of a pitching airfoil, *k* = 0.2, M = 0.5

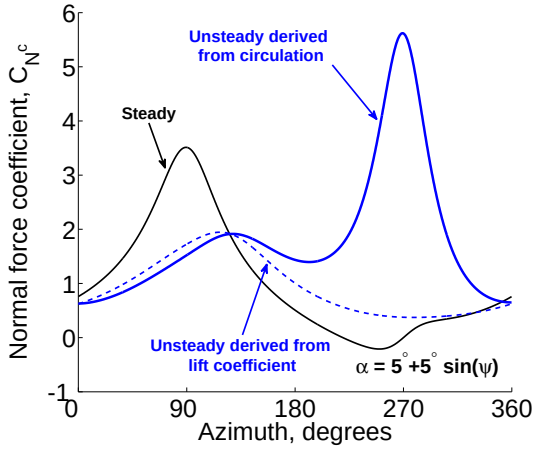

Fig. 4. Unsteady response of a pitching airfoil in a varying freestream, *k* = 0.21, M = 0.5(1 + 0.9sin(ψ)

4.2 Overview of Leishman-Beddoes Dynamic Stall Model

The Leishman-Beddoes semi-empirical dynamic stall model follows from the recursive formulation of the

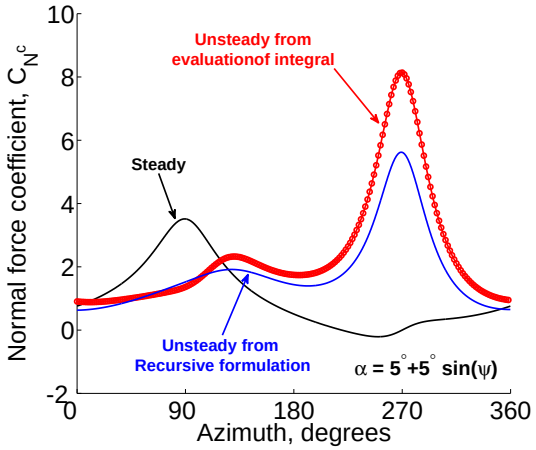

Fig. 5. Unsteady prediction error from recursive formulation at high Mach, *k* = 0.2, M = 0.5(1 + 0.9sin(ψ)

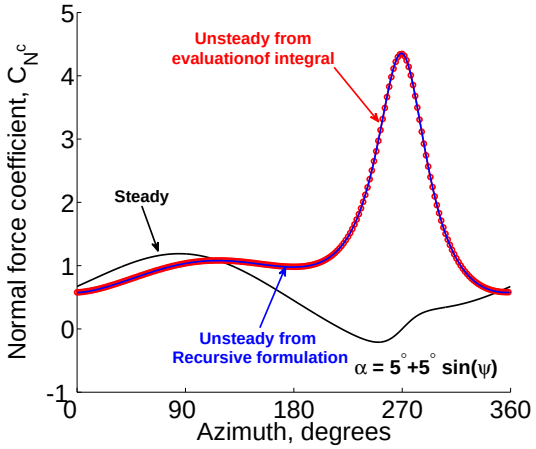

Fig. 6. Unsteady prediction error from recursive formulation at low Mach,*k* = 0.2, M = 0.2(1 + 0.9sin(ψ)

unsteady attached model. Dynamic stall occurs on helicopter rotors usually on the retreating side at high thrust and high speed conditions when there are large cyclic variations of pitch angle and high pitch rates. Distinguishing dynamic stall from static stall is a shedding of a significant concentration of vorticity from the aerodynamic leading edge, which moves along the chord and induces a strong suction pressure on the airfoil surface[27]. The pressure wave results in effective lift coefficients that exceed the static stall limits, a large nose-down pitching moment, and a large loss in lift (detachment) when the vortex leaves the airfoil trailing edge. Dynamic stall causes increased vibrations and can determine rotorcraft design limits. The Leishman-Beddoes model attempts to replicate the physics of this process while minimizing the number of empirical constants that cannot be generalized or determined from static airfoil behavior.

Summarizing the approach of Leishman[27], the approach is to determine the conditions for shedding the dynamic stall vortex, which are the conditions for leading edge separation. The leading edge pressure response, C_N^{le}, is assumed to be represented by the total normal force coefficient ($C_N^C + C_N^{NC}$). but with a first order time lag under unsteady conditions:

$$C_N^{le} = C_{N_n} - D_{p,n} \tag{3}$$

where

$$D_{p_n} = D_{p_{n-1}} e^{\Delta s/T_p} + (C_{N_n} - C_{N_{n-1}}) e^{\Delta s/(2T_p)}$$

where C_N^{le} is compared to $C_{N_{max}}$ (determined from moment stall from static airfoil data), which defines the onset of leading edge separation. An effective angle of attack, α_{eff}, can subsequently be found using the lift curve slope from airfoil data that represents the lead edge pressure condition.

$$\alpha_{eff} = \frac{C_N^{le}}{C_{n\alpha}} \tag{4}$$

The trailing edge separation point, f, is then modeled following the Kirchhoff approximation with coefficients determined from static airfoil lift behavior near stall. The separation point is further assumed to have an unsteady lag in response resulting in f_p. The unsteady separated normal force can then be determined from:

$$C_N = C_{n\alpha}(\alpha_E) Kn + C_N^{NC} \tag{5}$$

where

$$Kn = \frac{1}{4}(1 - \sqrt{(f')})^2$$

The constant coefficients in the preceding equations are generally a function of Mach number and airfoil shape, but most are determined from static airfoil data. The pitching moment is found in a similar way, but is always a function of the separated lift model.

The strength of the leading edge vortex at each time step is assumed to be the accumulation of excess circulation between the linearized lift and the separated lift, given by $C_{l\alpha}(\alpha_E)(1 - Kn)$. The total vortex strength, C_{NV_n}, is allowed to continuously decay as well as accumulate additional vorticity.

$$C_{NV_n} = C_{NV_{n-1}} e^{\Delta s/T_v} + (C_{V_n} - C_{V_{n-1}}) e^{\Delta s/(2T_v)} \tag{6}$$

During slow changes in lift, the leading edge vortex decays as fast as it accumulates, but when leading edge separation is triggered ($C_N^{le} > C_{N_{max}}$), the vortex is shed. Its speed along the chord is determined by a non-dimensional time, T_{vl}, which is Mach dependent. The pitching moment effect of the stall vortex is modeled as a movement in the vortex center of pressure from the quarter-chord to the trailing edge.

4.2 Adapting Leishman-Beddoes Dynamic Stall Model to Reverse Flow

4.2.1 Static airfoil coefficients

The Leishman-Beddoes airfoil specific coefficients are found from static airfoil stall data in the linear region of lift before stall and until just after stall. The key to the model is finding the coefficients of the Kirchhoff trailing edge separation model (generally a function of Mach number) that achieve a good fit with test data. The resulting fit is applicable to a narrow range of angles of attack. A general model to include reverse flow must have a piecewise fit in four regions; positive and negative angles of attack in forward and reverse flow. Outside of these regions, the model breaks down and the airloads must be smoothly collapsed onto static airfoil measurements.

4.2.1 Reverse flow transition

Under normal, forward flow, conditions, the Leishman-Beddoes separated and dynamic stall model is implemented following the standard dynamic stall model. Near the reverse flow boundary, the flow decelerates rapidly resulting in a large accumulation of excess circulation and there is no mechanism to transfer that circulation across the reverse flow boundary. The current approach assumes that all the circulation is shed instantaneously at the reverse flow boundary. Numerically this is achieved by setting all of the recursive terms (X_1, Y_1, etc) to zero. The practical advantage of this approach is that a decoupled dynamic stall model can be applied to each region. The implication of this approach is that the airfoil appears to start from rest within the reverse flow, with a ramp velocity. The large changes in angle of attack that occur at the transition have limited effect on airloads due to low dynamic pressures and instead the primary driver of unsteadiness is changing velocity.

4.2.1 Reverse flow model

The ramp in velocity is similar to an impulsively started flat plate. The results of Beckworth and Babinsky[31] and Ford and Babinsky[32] on the flow and circulation around an impulsively started flat plate provide some insight. The result in Fig. 7 (is adapted from[31]) shows the lift response to impulsive starts at 5° and 15° pitch angles. The 15° pitch angle is more representative of the pitch angles in the reverse flow (based on comprehensive analysis). The lift response grows rapidly and exceeds the static lift value within 0.25c of travel, then it decreases somewhat until near 1.75c. After 1.75c chord, the PIV (Fig. 7b) shows the

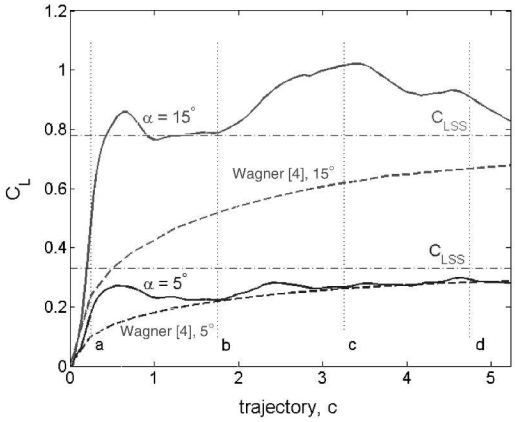

(a) C_l response for 5° and 15° pitch angles

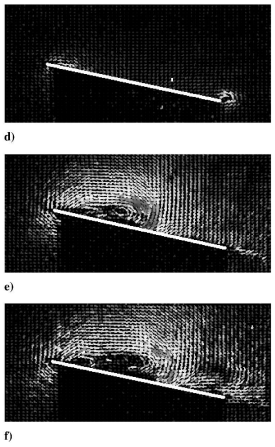

(b) PIV of 15° pitch flat plate after d)0.25c, e)1.75c and f)3.25c

Fig. 7. Lift and PIV response for impulsively started flat plate. Adapted from Beckworth and Babinsky[31].

leading edge vortex separating and this is accompanied by a growth in lift that continues until after 3.25c. The 5° lift response is qualitatively the same. Also shown, is that the total lift response does not follow the Wagner function. Ford and Babinsky[32] investigated the circulation strength of the leading edge vortex and trailing edge starting vortex and showed that they are each well approximated by the Wagner function. The implications of the two results is that the immediate C_l response is non-circulatory in nature. At some point thereafter, the LEV separates causing additional lift while it moves along the chord.

With this somewhat limited data set, the following approach is taken to predicting the dynamic stall response in the reverse flow.

1. The forward and reverse flows are completely decoupled. On entering and leaving the reverse flow region, the recursive storage variables are reset. Time within the reverse flow is measured in semi-chords s, based on the average velocity, and taking the absolute value.

2. Immediately thereafter, $s > 0$, the flow is assumed attached. Non-circulatory lift is neglected at the transition to avoid non-physically large impulses. The starting trailing edge vortex is neglected.

3. Following from the results of Refs.[31],[32], the lift is assumed to immediately attain the static lift values. This accounts for the rapid increase in lift as seen in the experiments for the impulsively started plate. Low dynamic pressures ensure that the error at small s is negligible.

4. The strength of the leading edge vortex, C_{NV}, grows following the Wagner function and decays in the same way as the Leishman-Beddoes model, but does not impact the lift.

5. At each time step, C_N^{le} is evaluated following Eq. (3), based on the unsteady lift.

6. Trailing edge separation is neglected.

7. The onset of shedding of the leading edge vortex is determined in the same way as the Leishman-Beddoes model, by comparing C_N^{le} to some $C_{N_{max}}$. When $C_{N_{max}}$ is exceeded, the vortex position is tracked in non-dimensional time by τ_v as starting at the geometric $^3/_4$ chord and moving towards the leading edge. The additional lift of the leading edge vortex is added to the static values of lift and decays rapidly.

8. The pitching moment due to the LEV is modeled as a movement of the center of pressure of the LEV from the $^3/_4$ chord to the leading edge as:

$$C_p = 0.5 - 0.75 sin(\frac{\pi}{2}\frac{\tau_v}{T_{vl}}) \quad (7)$$

where T_{vl} describes the speed at which the vortex moves along the chord.

9. Once the vortex leaves the vicinity of the airfoil ($\tau_v > 2T_{vl}$), a new stall LEV vortex is immediately allowed to detach if the conditions are met.

The empirically determined coefficients (not available from static airfoil data) used in the reverse flow are the same as those suggested by Leishman for the NACA0012 airfoil at low Mach numbers. The choice of $C_{N_{max}}$ is not obvious for the reverse flow airfoil. Under normal conditions, Leishman found that $C_{N_{max}}$ could correspond to the break in pitching moment or chord force. Recent results from Hodara et al.[33] for a NACA0012 airfoil oscillating in reversed flow suggest that the LEV separates earlier (lower relative angle

of attack) than in forward flow due to the sharp leading edge. A generalized criteria, including for varying Mach number, is not available. In this model, $C_{N_{max}}$ has been chosen to ensure the correct azimuthal onset of stall for the 9145 test point ($C_{N_{max}} = 1.0$), and not altered for the remaining cases.

4.2.1 Limitations of the reverse flow model

The implementation of this reverse flow stall model is an attempt to adapt the Leishman-Beddoes approach to the problem of dynamic stall in reverse flow. A robust and physics based model requires good experimental data for oscillating airfoils with varying freestream velocity, including flow reversal. Without these, a number of the coefficients are somewhat arbitrarily based on the original dynamic stall model for forward flow. The current approach is adapted through correlation with a single full-scale rotor test and the model is limited because of this. However, this is a first step towards identifying the role played by reverse flow dynamic stall on the loads of high speed rotorcraft using a comprehensive analysis.

5. RESULTS

Airloads correlation with tests

The normal force, pitching moment and chord force (scaled by Mach number squared) that result from the current implementation of the dynamic stall model are shown in Figs. 8 to 11 for the four test points considered. Each result shows the test data (**Test**: black dotted line), the UMARC predictions assuming quasi-steady and attached flow (**Steady**: blue dashed line) and the UMARC predictions including the adapted dynamic stall model (**DS**: red line).

Point 9125 - (Figure 8) In general, the unsteady aerodynamic model has no significant effect on the predictions of airloads on the advancing side and they remain similar to the quasi-steady aerodynamic case. In the reverse flow, the dynamic stall increment is seen clearly at 270° azimuth in the airloads and improved agreement with the measured test data. The dynamic stall model does not improve the overall prediction of the pitching moment in the reverse flow, but the absolute values are quite small. The chordwise force is generally poorly predicted by the analysis, but the dynamic stall addition seems reasonably well correlated.

Point 9145 - (Figure 9) For the μ = 0.6 case, the onset of dynamic stall on the retreating side is predicted. However, the magnitude of the lift and pitching moments are under-predicted by the model compared to the test data. The current model assumes that all the circulation on the blade is shed as the

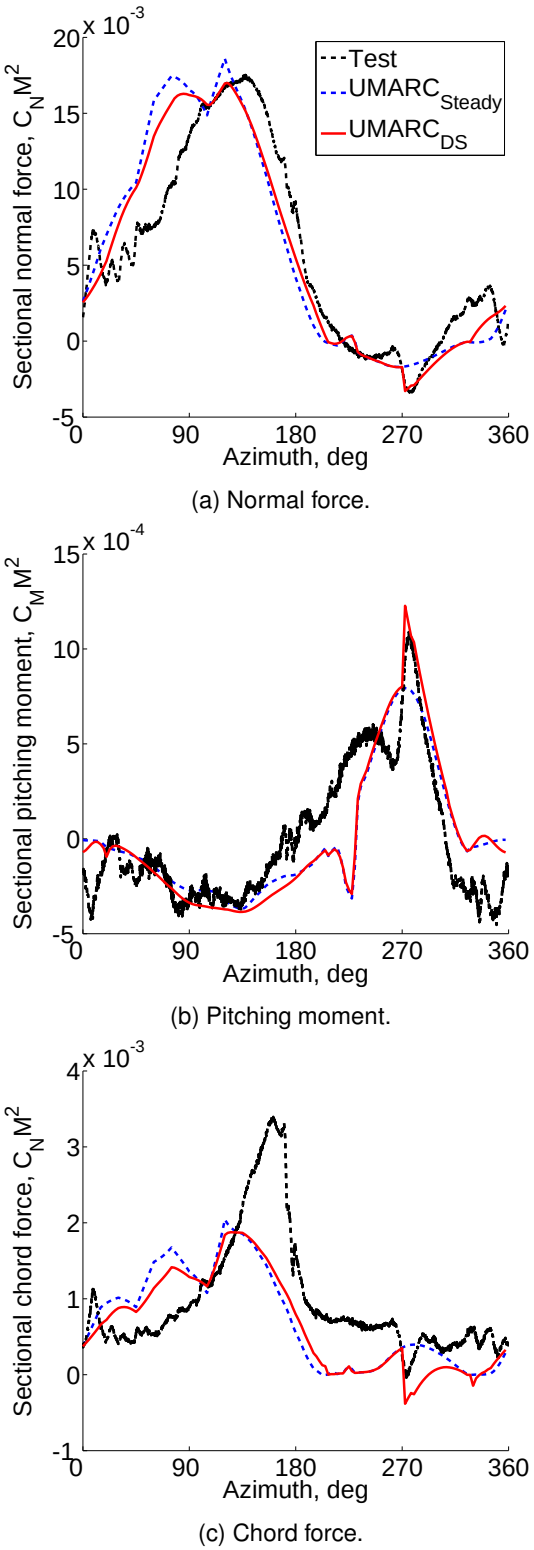

Fig. 8. Airloads at 22.5% radius for test point 9125 (μ = 0.4), showing effect of reverse flow dynamic stall model.

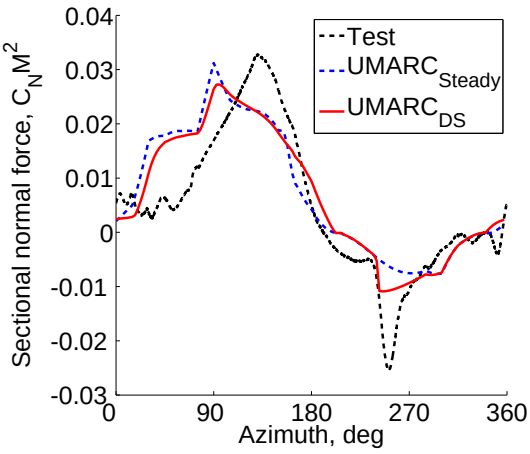

(a) Normal force.

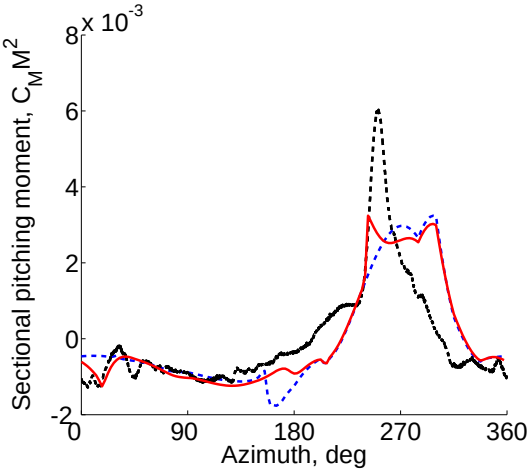

(b) Pitching moment.

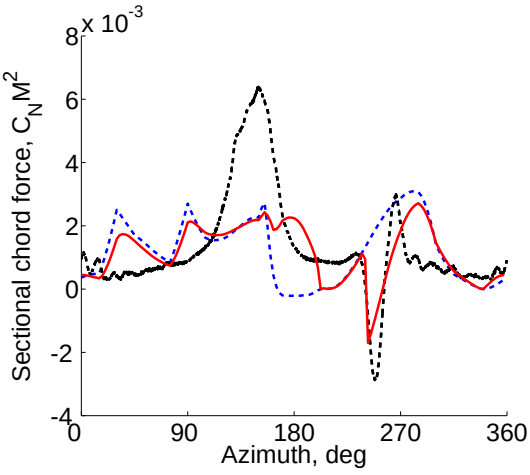

(c) Chord force.

Fig. 9. Airloads at 22.5% radius for test point 9145 (μ = 0.6), showing effect of reverse flow dynamic stall model.

stall vortex so the source of the under-prediction is not clear. The trimmed longitudinal cyclic for this case is -9.79°, which is close to the measured (-10°), suggesting similar aerodynamic states. However, this flow regime is extending the limits of the lifting line analysis and there may be three-dimensional flow effects that are important. The modeled pitching moment does not drop off after the predicted dynamic stall as is seen in the test and suggests that gross separation is not being modeled appropriately. The chordwise force impulse at the dynamic stall is reasonably well predicted. Finally for this case, the addition of the dynamic stall model has some effect on the advancing side, near 150° azimuth, where the stall seen in the steady predictions is avoided.

Point 9162 - (Figure 10) The μ = 0.9 case, the test data shows somewhat benign reverse flow airloads. The CFD analysis of this case predicted some lift and pitching moment (similar to the steady UMARC predictions). There is no sign of dynamic stall in the reverse flow. The dynamic stall model predicts two stall events at 240° and 300°, but there is no correlation with the test data. The reason for the large discrepancy (also seen in CFD) is unclear. One possibility is that the flow may be completely detached in the reverse flow.

Point 9175 - (Figure 11) At μ = 1.0, the dynamic stall model predicts three abrupt stall events, which decay rapidly and the airloads return to the steady lift values. The measured airloads also show three distinct potential stall events (205°, 240° and 312° azimuths), but there is no phase correlation. The unsteadiness in the measured airloads also seems to decay slower than the predictions. The measured normal force and pitching moment are advanced in azimuth compared to the predictions (both steady and dynamic stall), an there is lift produced over the reverse flow boundary when the tangential velocities are zero. The contribution of radial flow (large over the front of the rotor) may be important for unsteady loads and beyond the capability of the current analysis.

Figure 12 shows a map of the predicted onset and extent of dynamic stall for two high advance ratio cases (μ = 0.6 and 1.0). At μ = 0.6, a single strong vortex is predicted, which decays slowly across the entire reverse flow region. There is a strong impulse near 30% radius, which is caused by a wake interaction (the wake trailer originating from the same blade washes back on itself). At μ = 1.0, the shedding of the LEV is triggered more than once near the blade root. Figure 13 shows the predicted onset of the dynamic stall in terms of semi-chords traveled for the two cases. Also shown are estimates of the potential dynamic stall impulses from the test data (azimuth based on pitching moment, magnitudes are arbitrary). The first predicted stall occurs at 1.75–2.00

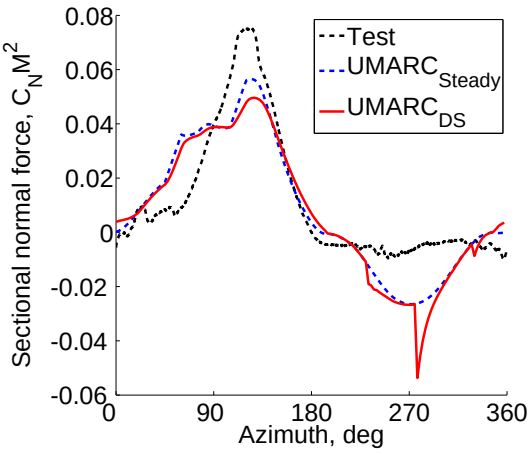

(a) Normal force.

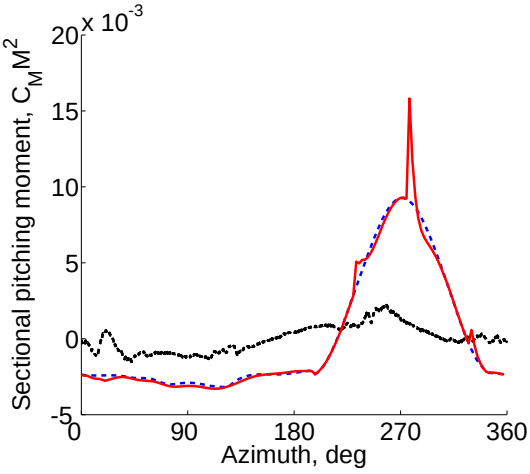

(b) Pitching moment.

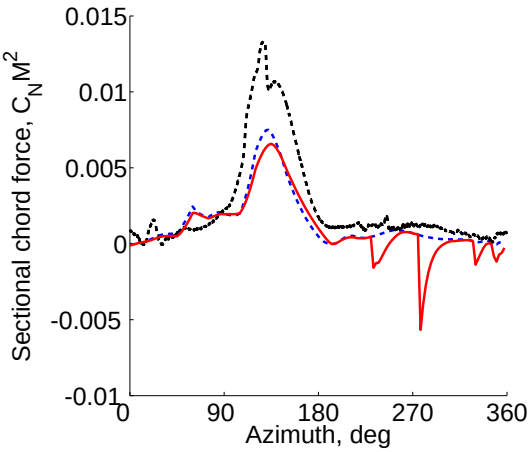

(c) Chord force.

Fig. 10. Airloads at 22.5% radius for test point 9162 (μ = 0.9), showing effect of reverse flow dynamic stall model.

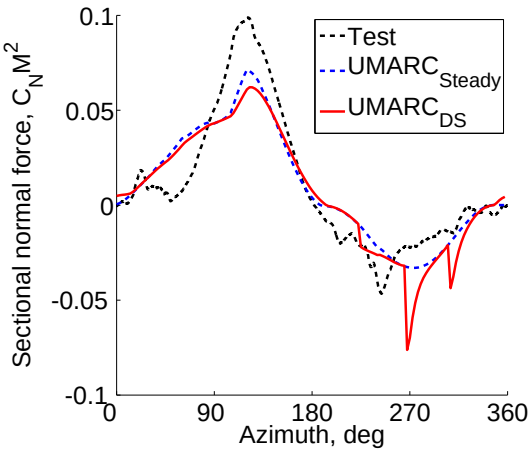

(a) Normal force.

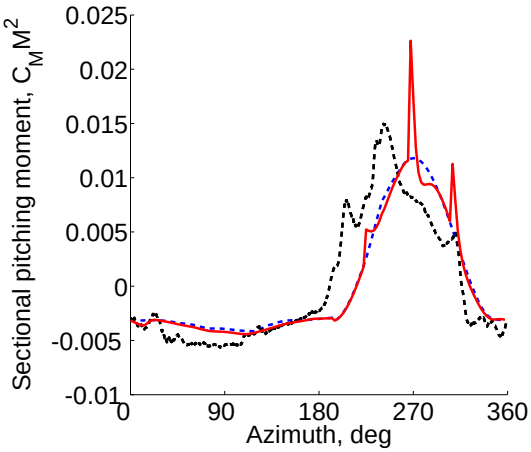

(b) Pitching moment.

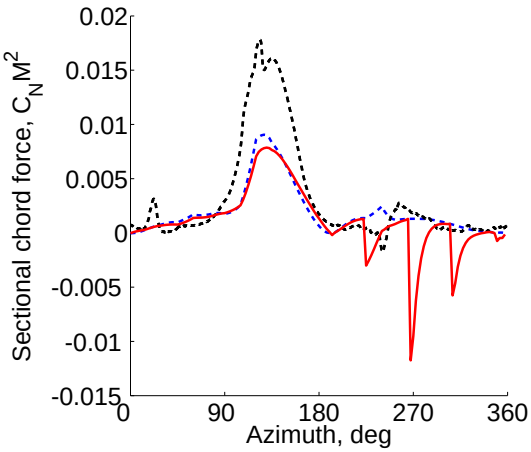

(c) Chord force.

Fig. 11. Airloads at 22.5% radius for test point 9175 (μ = 1.0), showing effect of reverse flow dynamic stall model.

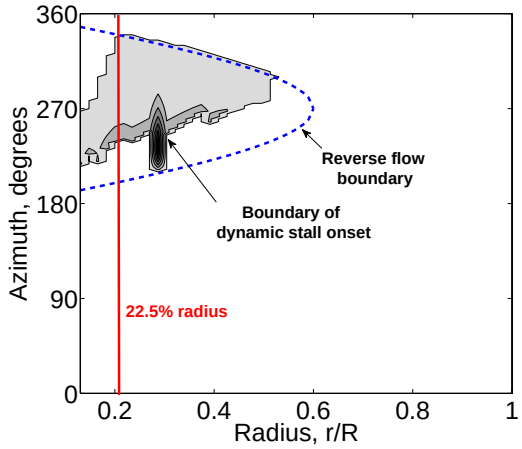

(a) Test point 9145 (μ = 0.6).

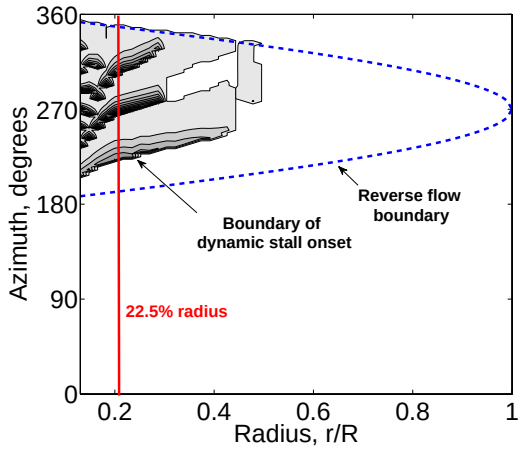

(b) Test point 9175 (μ = 1.0).

Fig. 12. Rotor map of dynamic stall onset within the reverse flow region.

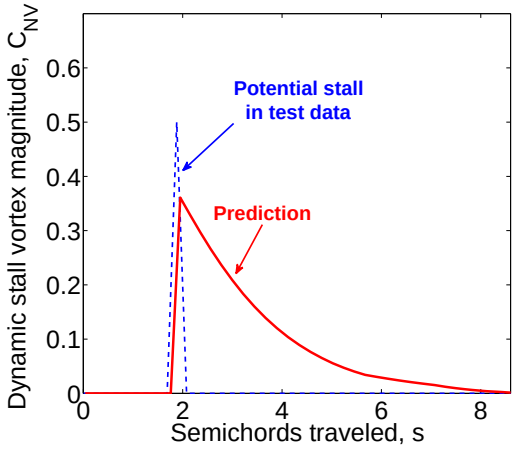

(a) Test point 9145 (μ = 0.6).

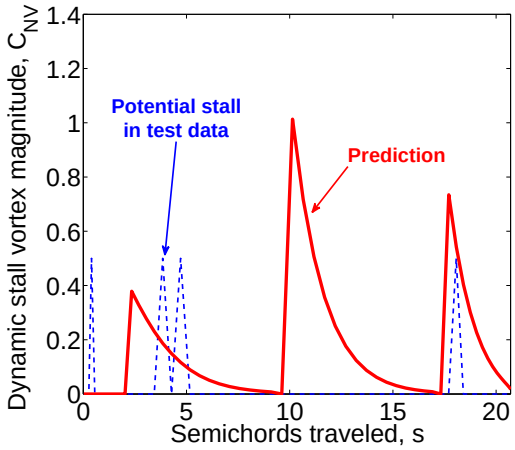

(b) Test point 9175 (μ = 1.0).

Fig. 13. Dynamic stall onset in terms of semichords traveled at 22.5% radius. Predictions (Red/solid) and estimated from test (Blue/dash)

semi-chords of travel for both cases, with poor agreement for the μ = 1.0 case. The frequency of the vortex shedding is currently controlled by the choice of the non-dimensional time constant T_{vl}, which defines the speed at which the vortex traverses the chord, the choice of $C_{N_{max}}$ and the flow speed (characterized by s). The present model does not vary T_{vl} or $C_{N_{max}}$ between the two cases. The higher advance ratio case promotes faster vortex progression, which allows a secondary vortex to shed, a phenomena present in the test data. To progress the model, these parameters must be characterized for the reverse flow airfoils.

6. CONCLUSIONS

This paper describes a new implementation of dynamic stall modeling for the reverse flow of high advance ratio rotorcraft, suitable for comprehensive analyses. The approach taken is to adapt the Leishman-Beddoes dynamic stall model with concepts from a flat plate in accelerating flow. The reverse flow unsteady aerodynamics are treated as though the airfoil is accelerated form rest at the reverse flow boundary, which allows the forward flow and reverse flow unsteady aerodynamics to be decoupled. The model is evaluated against airloads data from the reverse flow region of the UH-60A slowed rotor test at high advance ratios between μ = 0.4–1.0. The model predicts dynamic stall in the reverse flow in all cases, while the unsteady modeling has only a small effect on the advancing rotor. At lower advance ratios (μ = 0.4 and 0.6), the azimuth of dynamic stall is well predicted and the correlation with the measured airloads in the reverse flow is improved. At μ = 1.0, the model predicts multiple vortex shedding, which are present in the test, but the phase agreement is not satisfactory.

The following main conclusions are made.

1. The Leishman-Beddoes approach to modeling dynamic stall has been adapted to model dy-

namic stall-like vortex shedding in the reverse flow.

2. Four conditions from wind tunnel tests have been used to validate the model. At μ = 0.4 and 0.6, both test conditions show a single shed vortex, which is predicted by the model. The azimuth of the onset of dynamic stall is predicted, the magnitude prediction is good at μ = 0.4, but underpredicted at μ = 0.6. The dynamic stall model improves the reverse flow unsteady airloads predictions in normal and chord forces and pitching moments.

3. At μ = 0.9, the model predicts multiple dynamic stall events in the reverse flow, but the measured reverse flow airloads are benign. The analysis over-predicts the airloads magnitudes in the reverse flow. An explanation for the lack of lift or pitching moment in the measured airloads is unclear.

4. At μ = 1.0, the model predicts multiple dynamic stall events in the reverse flow and these are also seen in the test. The azimuthal onset of the dynamic stall is not well predicted. The test data suggests that an initial stall occurs immediately on entry to the reverse flow, not present in the model. The 3D flow, and radial flow in particular, may be important for the unsteady airloads predictions and are not modeled in the analysis.

5. The dynamic stall model assumes two dimensional flow. At the onset of reverse flow, the time history of the shed wake vanishes and the airfoil starts under steady conditions again. In the reverse flow, lift is allowed to develop following the Wagner function prediction for a flat plate under a ramp velocity. The primary source of circulation is from changing velocity instead of from large pitch changes.

6. In the current model, the criteria for the onset of dynamic stall, and that determines how often the vortex can be shed, are taken from the Leishman-Beddoes model for dynamic stall in forward flow. This choice is convenient, but controlled experiments of this type of stall are needed to update these.

7. Non-circulatory airloads may be important to predict the initial lift on the airfoil immediately after entering the reverse flow. These are neglected in the current approach.

Acknowledgments

This work is sponsored by the Israel Ministry of Defense, "Aeromechanics of Rotorcraft in High Speed Flight," Grant No. 4440560176 with technical monitor Dr. Avi Weinreb. Authors would like to thank Dr. Anya Jones and Andrew Lind for valuable discussions.

The authors would also like to acknowledge technical assistance from Dr. Anubhav Datta, as well as the support from Dr. Tom Norman of NASA, for providing the UH-60A test data.

References

[1]Wheatley, J. B. and Hood, M. L., "Full-Scale Wind-Tunnel Tests of a PCA-2 Autogiro Rotor," NACA Report No. 515, 1935

[2]Jenkins, J. L., "Wind-Tunnel Investigation of a Lifting Rotor Operating at Tip-Speed Ratios from 0.65 to 1.45," NASA TN D-628, 1965

[3]McCloud, J. L., Bibbers, J. C., and Stroub, R. H., "An Investigation of Full-Scale Helicopter Rotors at High Advance Ratios and Advance Ratios and Advancing Tip Mach Numbers," NASA TN D-4632, July 1968

[4]Charles, B. D., and Tanner, W. H., "Wind Tunnel Investigation of Semirigid Full-Scale Rotors Operating at High Advance Ratios," United States Army Aviation Material Laboratories TR 69-2, January 1969.

[5]Yeo, H., Johnson, W., "Optimum Design of a Compound Helicopter," *Journal of Aircraft*, Vol. 46, No. 4, July-August 2009, pp 1210–1221

[6]Floros, M., Johnson, W., "Performance analysis of the Slowed-Rotor Compound Helicopter Configuration, " *Journal of the American Helicopter Society*, Vol. 54, 2009, pp 022002 1–12

[7]Ormiston, R., "Rotor Aerodynamic Characteristics at High Advance Ratio Relevant to compound Rotorcraft," American Helicopter Society Future Vertical Lift Aircraft Design Conference, San Francisco, CA, January, 2012.

[8]Norman, T. R., Shinoda, P. M., Peterson, R. L., and Datta, A., " Full-scale Wind Tunnel Test of the UH-60A Airloads Rotor," American Helicopter Society 67^{th} Annual Forum, Virginia Beach, VA, May 3-5, 2011.

[9]Datta, A., Yeo, H., and Norman,. T. R., "Experimental Investigation and Fundamental Understanding of a Slowed UH-60A Rotor at High Advance Ratios," American Helicopter Society 67^{th} Annual Forum, Virginia Beach, VA, May 3-5, 2011.

[10]Potsdam, M., Datta, A., and Jayaraman, B., "Computational Investigation and Fundamental Understanding of a Slowed UH-60A Rotor at High Advance Ratios, " American Helicopter Society 68^{th} Annual Forum, Fort Worth, TX, May 1-3, 2012.

[11]Kottapalli, S., "Performance and Loads Correlation of a UH-60A Slowed Rotor at High Advance Ratios," American Helicopter Society Future Vertical Lift Aircraft Design Conference, San Francisco, CA, January, 2012.

[12]Ormiston. R., "Rotor Aerodynamic Characteristics at High Advance ratios Relevant to Compound Rotorcraft, " American Helicopter Society Future Vertical Lift Aircraft Design Conference, San Francisco, CA, January 18-20, 2012.

[13]Yeo, H., "Investigation of UH-60A Rotor Performance and Loads at High Advance Ratios, " *Journal of Aircraft*, Vol. 50, No. 2,March-April 2013, pp 576–589

[14]Bowen-Davies, G., and Chopra, I., "Investigation of the UH-60A Slowed Rotor Wind Tunnel Tests using UMARC," American Helicopter Society 69^{th} Annual Forum, Phoenix, AZ, May 21-23, 2013.

[15]Bowen-Davies, G., and Chopra, I., "Performance and Loads Correlation of the UH-60A Rotor at High Advance Ratios," 40^{th} European Rotorcraft Forum, Southampton, England, September 2-5, 2014.

[16]Bowen-Davies, G., and Chopra, I., "Validation of Rotor Performance and Loads at High Advance Ratio," Fifth Decennial AHS Aeromechanics Specialists Conference, San Francisco, CA, January 22-24, 2014.

[17]Bowen-Davies, G., and Chopra, I., 'Aeromechanics of a Slowed Rotor," AIAA, SciTech 2015, Kissimmee, Florida, January 5-9, 2015

[18]Berry, B., and Chopra, I., "Wind Tunnel Testing for Performance and Vibratory Loads of a Variable-Speed Mach-Scaled Rotor," American Helicopter Society 67^{th} Annual Forum, Virginia Beach, VA, May 3-5, 2011.

[19]Berry, B., and Chopra, I., "Performance and Vibratory Load Measurements of a Slowed-Rotor at High Advance Ratios," American Helicopter Society 68^{th} Annual Forum, Fort Worth, TX, May 1-3, 2012.

[20]Berry, B., and Chopra, I., "High-Advance Ratio Wind Tunnel Testing of Two Mach Scaled Rotors," American Helicopter Society 69^{th} Annual Forum, Phoenix, AZ, May 21-23, 2013.

[21]Berry, B., and Chopra, I., "High-Advance Ratio Wind Tunnel Testing of a Model Rotor with Pressure Measurements," American Helicopter Society Aeromechanics Specialists Conference, San Francisco, CA, January 20-24, 2014.

[22]Berry, B., and Chopra, I., "Slowed Rotor Wind Tunnel Testing of an Instrumented Rotor at High Advance Ratio," 40^{th} European Rotorcraft Forum, Southampton, England, September 2-5, 2014.

[23]Tran C. T. and Petot D., "Semi-empirical model for the dynamic stall of airfoils in view of the application to the calculation of responses of a helicopter in forward flight," Vertica 1981,(5), 3553.

[24]Petot D., "Differential equation modeling of dynamic stall," La Recherche Aerospatiale (English Edition) 1989, (5), 59–72.

[25]Chopra, I. and Bir, G., "University of Maryland Advanced Code: UMARC," American Helicopter Society Aeromechanics Specialists Conference, San Francisco, CA, January 1994.

[26]Bagai, A., Leishman, J.G., "Rotor Free-Wake Modeling using a Relaxation Technique - Including Comparisons with Experimental Data," *Journal of the American Helicopter Society*, Vol. 40, (2), April 1995, pp 29–41

[27]Leishman, J. G. and Beddoes, T. K., "A Generalized Method for Unsteady Airfoil Behaviour and Dynamic Stall using the Indicial Method," American Helicopter Society 42^{nd} Annual Forum, Washington, D.C., 1986.

[28]Leishman, J. G., Beddoes, T. S., "A Semi-Empirical Model for Dynamic Stall," *Journal of the American Helicopter Society*, Vol 34, (3), 1986, pp 3–17

[29]Leishman, J. G., "Validation of Approximate Indicial Aerodynamic Functions for Two-Dimensional Subsonic Flow," *Journal of Aircraft*, Vol 25, (10), 1987, pp 914–922

[30]Jose, A. I., Leishman, J. G., Baeder, J. D., "Unsteady Aerodynamic Modeling with Time-Varying Free-Stream Mach Number," American Helicopter Society 61^{st} Annual Forum, Grapevine, TX, June 1–3, 2005.

[31]Beckworth, R. M. H. and Babinsky, Holger, "Impulsively started Flat Plate Flow," Engineering Note, *AIAA Journal*, Vol. 46, (6), November - December 2009, pp 2186–2189

[32]Ford, Charles W. Pitt and Babinsky, Holger, "Impulsively started Flat Plate Circulation," Technical Note, *AIAA Journal*, Vol. 52, (8), August 2014, pp 1800–1802

[33]Hodara, J., Lind, A. H., Jones, A. R., Smith, M. J., "Collaborative Investigation of the Aerodynamic Behavior of Airfoils in Reverse Flow," American Helicopter Society 71^{st} Annual Forum, Virginia Beach, VA, May 5–7, 2015.